A new class of intermediate phases in non-crystalline films based on a confluent double percolation mechanism

2007 J. Phys.: Condens. Matter 19 455219

(http://iopscience.iop.org/0953-8984/19/45/455219)

IOP PUBLISHING JOURNAL OF PHYSICS: CONDENSED MATTER

J. Phys.: Condens. Matter **19** (2007) 455219 (10pp) doi:10.1088/0953-8984/19/45/455219

A new class of intermediate phases in non-crystalline films based on a confluent double percolation mechanism

Gerald Lucovsky[1] **and James C Phillips**[2]

[1] Department of Physics, North Carolina State University, Raleigh, NC 27695-8202, USA
[2] Department of Physics, Rutgers University, Piscataway, NJ 08854, USA

Received 13 September 2007
Published 24 October 2007
Online at stacks.iop.org/JPhysCM/19/455219

Abstract

Recent research results have suggested that double percolation processes play a significant role in the formation of intermediate phases (IPs) in non-crystalline thin films. One class of IP windows, involving *competitive double percolation*, occurs in binary As_xSe_{1-x} and Ge_xSe_{1-x} alloys and in the pseudo-binary $As_xGe_xSe_{1-2x}$ alloy. This IP window occurs over an 8–12% composition range. Transitions that define the IP window in the Ge–Se alloys involve a *competition* between the elimination of compliant local bonding dimer groups, e.g. Ge–Se–Se–Ge, at the expense of an increasing fraction of rigid local bonding monomer groups, e.g. Ge–Se–Ge. Compliant monomer group bonding defines the first window transition for an average number of bonding constraints/atom, $n_c = 3$; the second transition from rigid to stressed rigid occurs when the compliant monomer concentration drops below a concentration for percolation. A second class of IPs with significantly narrower composition windows, ∼1 to at most 3%, is proposed to explain experimentally determined IPs in chalcogenide alloys with halogen dopants; e.g. a-$Ge_{0.25}Se_{0.77-x}I_x$, where the IP window width is ∼1%. We suggest that this narrow window is determined by a *confluent coherent double percolation* process that includes (i) broken bond-bending constraints that minimize local bond strain, and (ii) a *percolation pathway* based on a second and complementary local bonding group. However, this second class of IPs is not supported by theory and modeling as yet, and as such our designation of this class of IPs must be regarded as more speculative. On the other had, it is significant that at least two other alloy systems, $Ge_2Se_2Te_5$ and pseudo-ternary Hf, Zr and Ti Si oxynitrides, display narrow regimes where bond constraint counting indicates local strain suppression, and where a second and larger bonding arrangement is present at the percolation limit.

1. Introduction

In non-crystalline thin films defect reductions can result from chemical bonding self-organizations that suppress percolation of macroscopic bond strain by creating *intermediate phases* (IPs) that have been identified by the reversibility of heat flow at glass transitions within the IP window [1, 2]. The chemical bonding self-organization within the IP windows of binary and pseudo-binary chalcogenide alloys such as As_xSe_{1-x} and Ge_xSe_{1-x}, and $As_xGe_xSe_{1-2x}$, and their S-substituted analogs, have been demonstrated to involve a *competitive double percolation* process involving the replacement of locally compliant *dimer* bonding groups such as Ge–Se–Se–Ge and As–Se–Se–As by locally rigid *monomer* bonding groups such as Ge–Se–Ge and As–Se–As, respectively [3–5]. This competitive double percolation is dominated by the compliant dimer bonding groups at the transition from floppy to rigid, at the first transition window from floppy to rigid, $x = 0.2$ in the Ge_xSe_{1-x} alloys and $x = 0.286$ in the As_xSe_{1-x} alloys [1, 3]. The composition and mean-field bond coordination, r_c, at this first transition are determined to coincide with a mean-field number of bond constraints/atom, n_c, equal to 3, the number of atomic degrees of freedom in a three-dimensional space-filling network. The alloy composition of the second transition from rigid to stressed rigid is determined by a competition between compliant dimer and rigid monomer bonding. As x is increased in either alloy, compliant dimer groups are replaced by more rigid monomer groups, until the concentration of dimer groups falls below a percolation limit [3]. Within the IP window, the stress is maintained at an effective value of $n_c = 3$, by chemical bonding self-organizations that continuously adjust to the competitive replacement process to minimize bond strain. The details of these self-organizations have not as yet been determined by theory or modeling, but are believed to be chemically specific, rather than generic in character [6].

We have proposed a qualitatively different IP window mechanism for alloy systems with a markedly narrower IP window that generally is not bracketed by floppy and stressed rigid regimes. This prototypical system for this second class of IP is the $Ge_{0.25}Se_{0.75-x}I_x$ alloy system. The IP window in this alloy, established by reversible heat flow measurements, occurs at a composition centered at $x \sim 0.16$, and with a window width of $\sim$0.01 [1]. At this alloy composition, two conditions are met at the same time: (i) the average number of bonding constraints/atom, $n_c = 3$, and (ii) a bonding arrangement, associated with a larger compliant group than the dimer groups addressed above, is at the percolation limit. Hence the descriptive, *confluent coherent double percolation* is deemed appropriate to contrast this window from the *competitive incoherent double percolation process* discussed above.

Before addressing the bonding in the three systems in section 3 that display the second class of IPs, we briefly review in section 2 two modifications to the two-component Lagrangian two-body bond-stretching and three-body bond-bending forces of the originally proposed semi-empirical bond constraint theory [3].

2. Force-field modifications to SEBCT

2.1. Broken bond-bending constraints

The concept of *broken* bond-bending constraints for tetrahedrally coordinated Si with two O and two Si bonding neighbors was first addressed by Lucovsky and Phillips in [7]. The local bonding is illustrated in figure 1(a). Symmetric three-atom bonding arrangements such as Si–Si–Si, and O–Si–O have are constrained at the tetrahedral angle of $\sim$110°. On the other hand, it is unlikely that the asymmetric O–Si–Si bond angles will be constrained to the same degree because the local *energy gaps* associated with O–Si and Si–Si bonds are different. If these gaps

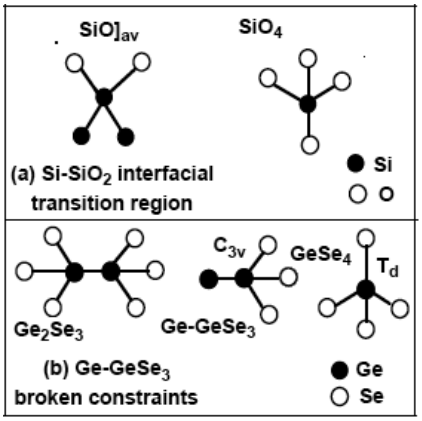

Figure 1. Schematic representations of tetrahedral bonding arrangements: (a) local bonding in SiO as discussed in [7]. This portion of the figure displays the average O_2–Si–Si_2 bonding as well as a reference Si–O_4 bonding. (b) The local Se_3–Ge–Ge–Se_3 bonding of the chemically ordered Ge_2Se_3 alloy, as well as the bonding of a completely symmetric Ge–Se_4 arrangement, T_d symmetry, and a reduced-symmetry Ge–Ge–Se_3 arrangement, C_{3v} symmetry.

are sufficiently different, the Pauling bonding resonance responsible for bond-bending forces is expected to be negligibly weak compared to the resonances responsible for the bond-bending forces associated with the symmetric Si–Si–Si and O–Si–O bond angles, and the constraints for the asymmetric bond angles will be removed from constraint counting and characterized as broken constraints.

Figure 1(b) gives a schematic representation of the Se_3–Ge–Ge–Se_3 bonding of the chemically ordered Ge_2Se_3 alloy [8], as well as the bonding of a completely symmetric Ge–Se_4 arrangement, and a reduced-symmetry Ge–Ge–Se_3 arrangement. Applying the same criterion to symmetric Se–Ge–Se and asymmetric Ge–Ge–Se bond angles, the bond constraints for symmetric geometries are retained, while for asymmetric geometries they are broken and therefore not counted [3, 9].

There are six bond angles for the completely symmetric $GeSe_4$ arrangement and each of these are symmetric, Se–Ge–Se. This in turn corresponds to five bonding constraints/Ge atoms that are associated with the five independent bond angles. In contrast, there are three symmetric Se–Ge–Se bonding arrangements, and three asymmetric Ge–Ge–Se arrangements for the reduced-symmetry Ge–Ge–Se_3 tetrahedron. The number of bond-bending constraints is reduced from five for the symmetric Ge–Se_4 bonding to $\sim$2.5 for this symmetric Ge–Ge–Se_3 bonding. This reduction is based on the application of mean-field constraint counting, or equivalent to a resonating sixth bond angle that can be either symmetric or asymmetric so that on average of 2.5 constraints are maintained and 2.5 are broken.

2.2. Repulsive bonding constraints

Additional constraints are associated with the relatively strong repulsive forces between the electrons in (i) lone-pair orbitals on nearest-neighbor network As and Se atoms in As–Se and Ge–As–Se alloys, and (ii) lone-pair Se orbitals and terminal I atoms in Ge–Se–I alloys [3]. Figure 2(a) includes schematic representations of the bonding arrangements in As_xSe_{1-x} alloys. The mean-field bonding at the compound composition, As_2Se_3, is shown in a plan view representation with three different geometric arrangements for the lone-pair electrons on the As atoms, in (i) *up–up*, (ii) *up–down* and (iii) *down–down* geometries. Figure 2(b) indicates the mean-field bonding in the As_2Se_5 ($r_c = 2.29$, $x_c = 0.286$) composition which is present at the transition into the IP window [1, 3].

The importance of the repulsive forces involving non-bonding pairs on two and three coordinated network atoms, and on halogen terminators, has been understood in molecular

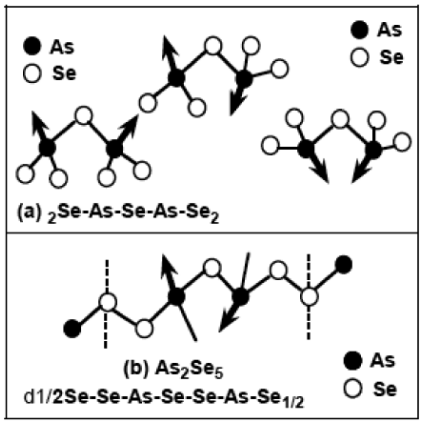

Figure 2. Plan-view schematic representations of bonding arrangements in As_xSe_{1-x} alloys. (a) The mean-field bonding at the compound composition, As_2Se_3, indicating three different geometric arrangements of the lone-pair electrons on the As and Se atoms: (i) up–up, (ii) up–down and (iii) down–down. (b) The mean-field bonding in the As_2Se_5 ($r_c = 2.29$, $x_c = 0.286$) composition. The solid arrows represent the orientations of the As lone-pairs. The lone-pairs on the Se atoms are normal to the plane of the diagram.

bonding chemistry for more than 30 years, and is integrated into the valence shell electron pair repulsion (VSEPR) model [10, 11]. The VSEPR model has been used to predict the *shapes of small molecules*, generally with from three to seven atoms, and identifies the significant contributions of non-bonding lone-pair electrons in contributing to asymmetric molecular structures such as XeF_6. This model is based on total energy calculations, in particular on an observation that bonding arrangements between the two-electron sigma (σ) and pi (π) bonds and non-bonding lone-pairs of near-neighbor atoms in a molecule will adopt a geometry in which the distance between the electron pairs in σ- and π-bonds and the lone-pair electrons is optimized by reducing repulsive interactions.

Applied to network non-crystalline solids, this allows us to identify bonding constraints that go beyond the elementary two-body bond-stretching and three-body bond-bending forces of the original formulation of the SEBCT. This is based on an analogy between distortions in molecules that include non-bonding pairs, and additional constraints in non-crystalline network solids that include non-bonding lone-pairs on two different atomic constituents, e.g. As and Se in As_xSe_{1-x} and $Ge_xAs_ySe_{1-x-y}$ alloys, and lone-pairs on one atomic constituent and a terminal halogen atom, e.g. Se and I, respectively, in $Ge_{0.25}Se_{0.75-x}I_x$. One additional constraint/atom will be added to each pair of like atoms involved in a lone-pair repulsion such as, for example, the pairs of As atoms separated by one Se (or S) atom. Because of the higher density of non-bonding electrons on halogen atoms compared with As, the number of constraints for each halogen atom will be increased as the square root of the number of non-bonding pairs, or from 1 to 1.5 constraints/halogen atom.

3. The a-$Ge_{0.25}Se_{0.77-x}I_x$ alloy system

Based on heat flow measurements, the IP window in this ternary alloy is very narrow, extending from approximately $x_c(1) \sim 0.165$ at the threshold from floppy to rigid, to $x_c(2) \sim 0.155$ at the second threshold from rigid to stressed rigid, with $\Delta x_c \sim 0.01$, and about 8–12 times smaller than for the binary and pseudo-binary chalcogenide alloys with competitive double percolation,

i.e. As_xSe_{1-x} and Ge_xSe_{1-x}, and $As_xGe_xSe_{1-2x}$ addressed [1, 3]. These alloy concentrations correspond respectively to mean-field average bonding coordinations of $r_c(1) = 2.335$ and $r_c(2) = 2.345$ [1], both of which fall below the first transition of the Ge–Se alloy system, and additionally, are very close to the experimentally determined values from the reversible heat flow measurements.

In order to estimate the values of $n_c(1)$ and $n_c(2)$ that correspond to the experimentally determined values of $x_c(1)$ and $x_c(1)$ it is necessary to take into account (i) broken constraints on the Ge atoms which are terminated by I atoms, as well as (ii) additional constraints on Se atoms which are due to repulsions between their lone-pair π-state and the non-bonding pairs on the terminal I atoms. This asymmetric tetrahedral arrangement, I–Ge–Ge_3, means that there are broken bond-bending constraints on 16.5% of the Ge atoms ($n_c(\text{bnd}) \sim 2.5$) and full bonding constraints on 8.5% ($n_c(\text{bnd}) = 5$). The value of $n_c(\text{Se})$ is increased by one constraint to include interactions between the Se lone-pairs and the non-bonding lone-pair electrons on the terminal I atoms. This adds ∼1 constraint for 30% of the Se atoms, so that the average number of Se constraints is increased from 2 to 2.3. Finally, the number of constraints on the terminal I atom consists of 0.5 stretching constraints (for a terminal atom); 1.5 additional constraints are added for the repulsive interactions with the Se atom non-bonding pairs. Proceeding in this way, the average number of constraints per atom at the floppy-to-rigid transition is estimated in the following calculation: $n_c(1) \sim 0.165(4.5) + 0.085(7)$ for Ge, 0.585(2.3) for Se, and 0.165(2) for I, so that $n_c(1) \sim 3.01$. The number of constraints/atom for the rigid-to-stressed transition is estimated by the same constraint counting, and $n_c(2) \sim 3.04$.

Additionally, it is important to recognize that the concentration of I atoms within the window is ∼16%, essentially at the percolation limit for macroscopic strain relief associated with a larger structure unit, which we take to be an asymmetric tetrahedral group, I–Ge–$Se_{3/2}$. Therefore within the IP window there is a confluence of (i) broken bond-bending constraints and additional constraints on the Se and I atoms due to near-neighbor repulsions which yield values of $n_c \sim 3$, and (ii) the percolation of a larger structural unit, I–Ge–$Se_{3/2}$, which reduces macroscopic strain as well. This confluence characterizes the second class of IP windows, and embraces the descriptive, confluent coherent double percolation. Finally, figures 3(a) and (b) include plots of the IP windows for the $Ge_{0.25}Se_{0.75-x}I_x$ alloys that are compared with alloys in which there is competitive incoherent double percolations, with the focus of the respective IP window widths.

4. The $Ge_2Sb_2Te_5$ alloy

This short summary includes (i) *a critical evaluation* of the extended x-ray absorption fine structure (EXAFS) data, and (ii) provides *increased insight* into the significance of the over-coordinated and positively charged Te atoms in facilitating the photon-assisted phase change. These charged defects are proposed as precursor states for crystallization into the face-centered cubic (fcc) rock salt structure that is important for the optical property changes in read/write (RW) DVD discs [9, 12, 13].

The EXAFS data for each of the atomic species, Ge, Sb and Te shows more than one spectral feature [13]. The analyzed results, primarily bond lengths, and coordination have been converted into a bonding model that is consistent with the local coordinations, and is represented by the *symbolic description* in equation (1):

$$Ge_2Sb_2Te_5 = Ge_2Te_3 + Sb_2Te_3 + 16\% \text{ over-coordinated Te–}Te_3^{(+1)}. \quad (1)$$

Additional studies reported at International Conference on Amorphous and Nano-Crystalline Semiconductors (ICANS-22) this year have supported this model, in particular the

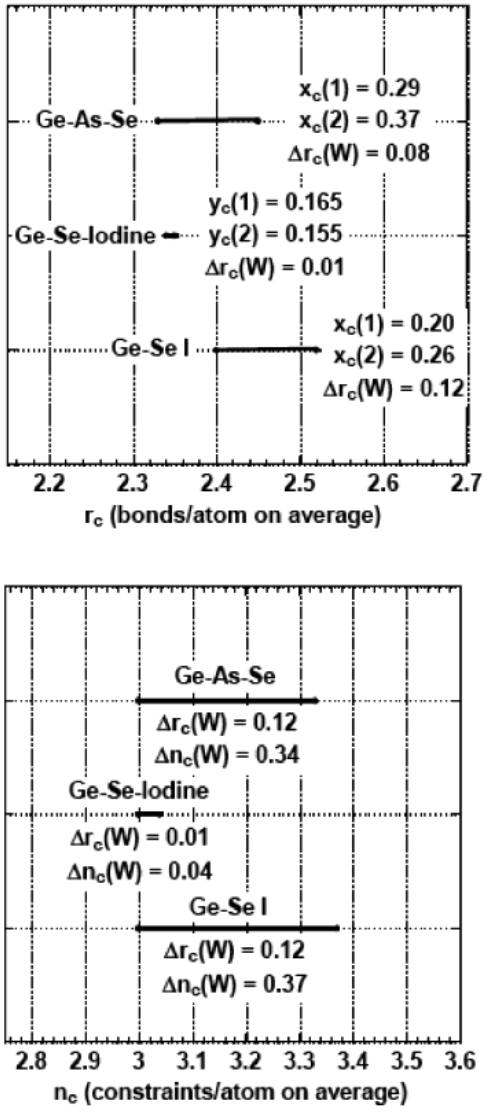

Figure 3. Schematic representation of IP regimes in the Ge_xSe_{1-x}, As_xSe_{1-x} and $Ge_{0.25}Se_{0.75-x}I_x$ alloy systems as functions of (a) r_c and (b) n_c.

importance of the Ge_2Te_3 bonding and the Te over-coordination, which has been correlated with the shorter Sb–Te bond length as well [12, 13]. Figure 4 indicates the local bonding arrangements in equation (1). More importantly, the $Ge_2Sb_2Te_5$ composition is likely to be an intermediate phase or IP; i.e. the average number of bonding constraints/atom, adjusted for broken bond-bending constraints on the Ge atoms in the Ge–Ge–Se_3 distorted tetrahedral arrangements, is $n_c \sim 3$. Equally importantly, the composition lies on several tie lines in the Ge–Sb–Te ternary phase field, in which its immediate neighbors also have values of $n_c \sim 3$.

The compositions $Ge_2Se_2Te_6$ and $Ge_2Se_3Te_7$ have values of $n_c \sim 3$, but their respective stoichiometries does not require over-coordinated Te atoms. Analysis of EXAFS data in [13] supports the absence of over-coordinated, positively charged Te. Over-coordinated bonding correlates with the sharpness of the optically driven transition from non-crystalline to fcc, indicating that this bonding defect arrangement is important in facilitating this technologically

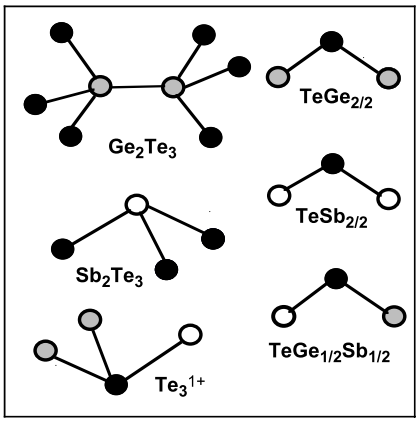

Figure 4. Plan-view schematic of local bonding arrangements in $Ge_2Sb_2Te_5$ RW memory layers. Solid black circles are Te; open white circles are Sb; and open gray circles are Ge.

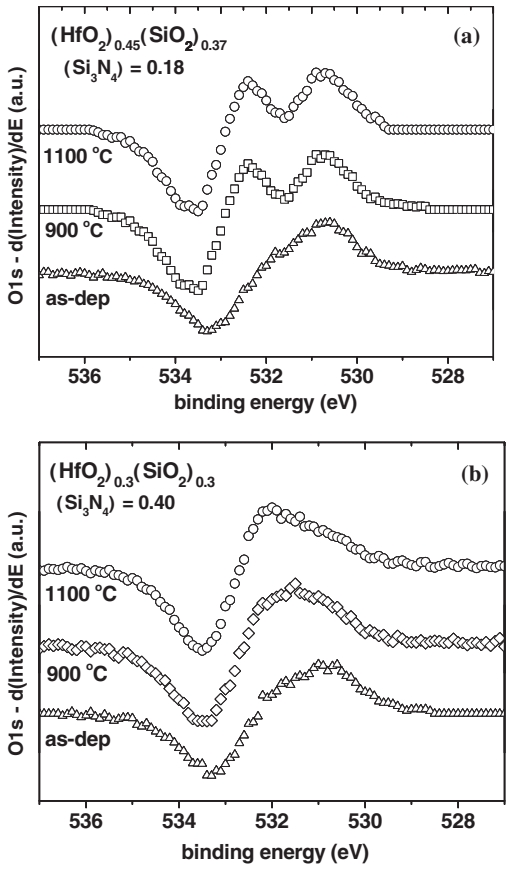

Figure 5. Hf Si oxynitrides derivative XPS O1s core level: (a) low Si_3N_4, 18%, showing chemical phase separation; (b) high Si_3N_4 content, 40%, no chemical phase separation.

significant transition [9, 12]. In this regard it is important to note that the concentration of over-coordinated Te is 16.7%, and that a larger structural unit consisting of the three-fold coordinated Te and its nearest Ge and/or Sb atoms is sufficient to provide relief of macroscopic strain as well. Hence the conditions for are met for a limited number of compositions centered at $Ge_2Sb_2Te_5$, and the resulting IP, which is yet to be verified by other experiments, e.g. reversible heat flow, may indeed be a second example of confluent coherent double percolation.

5. The Hf, Zr, and Ti Si oxynitride alloys

This section also identifies confluent coherent double percolation bonding in $(Hf(Zr, Ti)O_2)_{0.3}$ $(SiO_2)_{0.3}(Si_3N_4)_{0.4}$ pseudo-ternary alloys. A prerequisite for this second class of confluent double percolation is that the alloy contains three or more atomic species. In sections 4 and 5, we argued that this double percolation effect occurred for a relatively narrow range of alloy compositions, 1–2%, in the ternary phase diagrams of Ge–Se–I and Ge–Sb–Te. This section identifies a qualitatively similar behavior in quaternary alloys containing a group IVB transition metal, Hf, Ti or Zr (or a combination of two of these transition metals, Hf and Ti), Si, O and N. The focus will now be on the Hf Si oxynitride alloys. The previously reported spectroscopic studies, and the supporting electrical data to confirm low densities of defects, are better described in terms of a pseudo-ternary alloy characterization instead of random bonded quaternary alloy.

There is a relatively narrow composition range for Ti, Zr, Hf and mixed Ti, Hf Si oxynitride alloys that are stable against chemical phase separation (CPS) to temperatures $>1000\,^{\circ}C$ (see figure 4) [14]. However, the Hf Si oxynitrides are particularly interesting for applications as gate dielectrics on either Si or Ge substrates [15]. Analysis of electrical measurements of capacitance versus voltage (C–V) and current versus voltage (I–V) performed on films with a physical thickness of approximately 4 nm and incorporated on n-type and p-type Si and Ge substrates in conventional MOS test structures have indicated (i) static dielectric constants, k_{static}, $\sim$12 (three to four times higher than SiO_2), (ii) defect levels and reliability comparable to SiO_2 [16], and (iii) tunneling leakage currents of $<10^{-6}$ A cm^{-2} for 1 V bias, with at an effective oxide thickness (EOT) of $\sim$1.3 nm, as normalized to the dielectric constant of SiO_2. These properties are correlated with a pseudo-ternary alloy composition of $(HfO_2)_{0.3}(SiO_2)_{0.3}(Si_3N_4)_{0.4}$ (uncertainty, $\delta \sim 0.02$) which we have characterized as an Si_3N_4-rich composition. In marked contrast, alloys with reduced Si_3N_4 content between 15 and 25% Si_3N_4 and equal concentrations of SiO_2 and HfO_2 are not stable, and chemically phase separate in SiO_2 and HfO_2, as detected by derivative x-ray photoelectron spectroscopy, as shown in figure 5 [14, 15].

These compositions are not associated with a crystalline phase, and occupy a very limited portion of the respective ternary phase diagrams; additionally, these alloy compositions correspond to a confluent double percolation IP regime as well. This issue, first addressed with respect to the Hf Si oxynitride phase, and this analysis is then reinforced with a discussion of the $Ge_{0.25}Se_{0.75-x}I_x$ alloys discussed above. Figure 6 indicates the bonding arrangements in the high-Si_3N_4 content Hf Si oxynitride alloys, as deduced from spectroscopic data, primarily O K_1 and N K_1 edge spectra that have been differentiated to confirm Hf d-state splittings.

The two criteria for a confluent double percolation IP regime are (i) the number of constraints per atom must be approximately three, and equal to the number of degrees of freedom on average in a three-dimensional (3D) network to ensure minimal local bond strain, and (ii) there must be a percolation pathway for strain relief on a large scale. Applying the same constraint counting as discussed above, and including broken bending constraints on Si, Hf, and O atoms, this is associated respectively with (a) a reduction in local site symmetry in Si associated with a chemically ordered bonding in figure 6, (b) elimination of bending constraints at the tetrahedrally bonded Hf sites due to a significant degree of ionic bonding character, $\sim$0.7, on the Pauling scale, and (c) removal of the Si–O–Zr bond-bending constraint due to the asymmetric character of the bonding arrangement and, finally, (d) removal of the Si–O–S bond-bending constraint due to a large bond angle at the Si–O–Si bonding sites. This leads to a value of $n_c = 3.08$, which is sufficiently close to 3 for essentially complete relaxation of local bond strain on average. The percolation pathway is provided by the fraction of Hf atoms

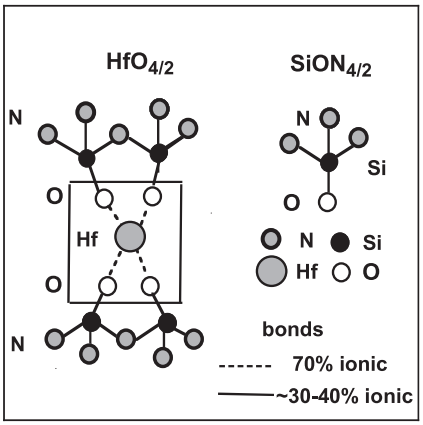

Figure 6. Bonding arrangements of Si and Zr in the high-Si_3N_4 content Hf Si oxynitride alloys, as deduced from spectroscopic data.

on four-fold coordinated sites; this is 1/6, and therefore it meets the Zallen–Scher criterion ([17], and references therein). For alloy compositions with higher Si_3N_4 content, e.g. below the percolation limit for global strain relief (for example, for a 50% Si_3N_4 fraction), the ratio of Hf/Si is 1/8 or 12.5%, 16.7%. Additionally, these films show a loss of N after an anneal at 900 °C, which is accompanied by CPS into SiO_2 and HfO_2. Similarly for smaller Si_3N_4 content, e.g., 25%, the alloy films also show CPS into SiO_2 and HfO_2, but with no loss of N, suggesting that the SiO_2 detected by O 1s XPS may have a significant N-content as well.

6. Summary and conclusions

This article has addressed the compositional widths of intermediate phase (IP) regimes in several binary and ternary chalcogenide alloys, Ge_xSe_{1-x}, As_xSe_{1-x}, $As_xGe_xSe_{1-2x}$, $Ge_{0.25}Se_{0.75-x}I_x$, and $Ge_2Sb_2Te_5$, as well as pseudo-ternary transition metal (Ti, Zr, Hf and Ti/Hf) Si oxynitrides, and $Ge_2Sb_2Te_5$. It has differentiated, for the first time, between two different types of IP window widths that herald different types of double percolation processes. This has been accomplished by extending the restricted valence force-field approach of conventional SEBCT by including broken bonding-bending constraints that derive from asymmetric bonding triads, e.g. Ge–Ge–Se, in contrast to symmetric triads, Se–Ge–Se, and introducing a new class of bonding constraints that are associated with many-body electron repulsions that involve either occupied lone-pair orbitals on respectively two-fold and three-fold coordinated chalcogens, S, Se or Te, and pnictides, P, As or Sb, and also terminal halogen atoms, such as F, Cl, Br and I that are qualitatively different to H and D terminators.

Double percolation effects have been shown to play an important role in the formation of intermediate phases (IPs), and two qualitatively different types of IP have been identified. The first class is based on competitive double percolation and occurs in binary and pseudo-binary alloys, e.g. (i) Ge_xSe_{1-x} and As_xSe_{1-x}, and $As_xGe_xSe_{1-2x}$, respectively [3]. The IPs have been designated competitive incoherent double percolation (CIDP-IPs), since they involve a compositionally dependent competition between compliant dimer local bonding arrangements, e.g. Ge–Se–Se–Ge or As–Se–Se–As, and rigid monomer local bonding arrangements, e.g. Ge–Se–Ge and As–Se–As. The Ge_xSe_{1-x} and As_xSe_{1-x} IP windows are consistent and have prompted the definition of a *competitive incoherent double percolation IP* window: (i) the

transition between floppy and rigid at the beginning of the IP window is marked by $n_c(1) = 3$; and (ii) the second transition, between rigid and stressed rigid, is determined by a concentration at which the compliant phase ceases to percolate, and at which the rigid phase is also above a limit for percolation. The transition into the IP window is consistent with percolation of one of the two competitive 'back-bone' inequivalent bonding arrangements; in this instance, the compliant one is clearly dominant and well above the percolation limit at this first transition. On the other hand, the termination of the IP range is more abrupt, and occurs when the compliant bonding environment drops below the percolation limit. IP windows are typically of the order of $\Delta x \sim 0.1$ or 10% in alloy composition space.

The second class of intermediate phases occurring primarily in ternary and quaternary alloys has been designated in this article as confluent coherent double percolation IPs to emphasize that is driven by chemical bonding self-organizations resulting in a *simultaneous occurrence* or *confluence* of (i) broken bond-bending constraints that minimize local bond strain, and (ii) a percolation path that minimizes macroscopic strain. Examples of this second class of IPs include two chalcogenide alloys, $Ge_{0.25}Se_{0.75-x}I_x$, and $Ge_2Sb_2Te_5$, as well as pseudo-ternary transition metal (Ti, Zr, Hf and Ti/Hf) Si oxynitrides. These IPs occur in a much narrower region of r_c-defined space with IP window widths of <0.05 in composition space, as compared to similar IP window widths for the competitive incoherent double percolation alloys that are typically at least 0.08 wide and extend to widths of more than 0.1.

Acknowledgments

This work was supported in part by the Office of Naval Research, the Semiconductor Research Corporation, and the Air Force Office of Scientific Research. The authors acknowledge S Lee, J P Long, J L Whitten, H Seo, L B Fleming and M D Ulrich, all from North Carolina State University, and J Lüning of Stanford Synchrotron Research Laboratory for their contributions to the research results of this paper.

References

[1] Wang F and Boolchand P 2004 *Non-Crystalline Materials for Optoelectronics* ed G Lucovsky and M Popescu (Romania: INOE) chapter 2 p 15
[2] Boolchand P, Lucovsky G, Phillips J C and Thorpe M F 2005 *Phil. Mag.* **85** 3823
[3] Lucovsky G and Phillips J C 2007 *J. Phys.: Condens. Matter* **19**
[4] Levon K, Margolina A and Patashinsky A Z 1993 *Macromolecules* **28** 4061
Gubbels F, Blacher S, Vanlathem E, Jerome R, Deltour R, Brouers F and Teyssie P 1995 *Macromolecules* **28** 1559
[5] Moraal H 1995 *J. Phys. A: Math. Gen.* **28** 2745
[6] Sartbaeva A, Wells S A, Huerta A and Thorpe M F 2007 *Phys. Rev.* B **75** 224204
[7] Lucovsky G and Phillips J C 2004 *Appl. Phys.* A **78** 453
[8] Lucovsky G, Nemanich R J and Galeener F L 1977 *Proc. 7th Int. Conf. on Amorph. Liquid Semconduct. (Univ. Edinburgh, Edinburgh, 1977)* p 130
[9] Lucovsky G G, Baker D A, Paesler M A and Phillips J C 2007 *J. Non-Cryst. Solids* **353** 1713
[10] Cotton F A and Wilikinson G 1972 *Advanced Inorganic Chemistry* 3rd edn (New York: Interscience) chapter 3
[11] Shriver D and Atkins P 1999 *Inorganic Chemistry* 3rd edn (New York: Freeman) chapter 3
[12] Baker D A, Paesler M A, Lucovsky G, Agrawal S C and Taylor P C 2006 *Phys. Rev. Lett.* **96** 25501
[13] Paesler M A, Baker D A, Lucovsky G and Taylor P C 2007 *J. Non-Cryst. Solids* at press
[14] Lucovsky G, Seo H, Lee S, Fleming L B, Ulrich M D, Lüning J, Lysaght P and Bersuker G 2007 *Japan. J. Appl. Phys.* **46** 1899
[15] Rayner G B, Kang D and Lucovsky G 2003 *J. Vac. Sci. Technol.* B **21** 1783
[16] Lucovsky G, Seo H, Lee S, Fleming L B, Ulrich M D and Lüning J 2007 *Microelectron. Eng.* **86** 2350
[17] Zallen R 1983 *The Physics of Amorphous Solids* (New York: Wiley–Interscience) chapter 7